Phosphorylation of Bni4 by MAP kinases contributes to septum assembly during yeast cytokinesis.

Jacqueline Pérez[1], Irene Arcones[1], Alberto Gómez[1], Verónica Casquero[1] and César Roncero [1].

(1) From the IBFG and Departamento de Microbiología and Genética. CSIC/Universidad de Salamanca

IBFG, Salamanca Spain, 37007

Running title: The overlapping action of protein kinases in septum assembly during cytokinesis.

Keywords: Cytokinesis, Septum assembly, MAP kinase

ABSTRACT

Previous work has shown that the synthetic lethality of the *slt2*Δ*rim101*Δ mutant results from a combination of factors, including improper functioning of the septum assembly machinery. Here we identify new multicopy suppressors of this lethality including Kss1, Pcl1 and Sph1, none of which seems to be linked to the upregulation of chitin synthesis. Characterization of the suppression mediated by Kss1 showed that it is independent of the transcriptional response of the CWI signaling response, but efficiently restores the Bni4 localization defects produced by the absence of Slt2. Accordingly, Bni4 interacts physically with both kinases, and its levels of phosphorylation are reduced in the *slt2*Δ mutant but increased after Kss1 overexpression. Using an assay based on hypersensitive cells of the *cdc10-11* mutant, we have pinpointed several MAP kinase phosphorylatable residues required for Bni4 function.

Our results, together with a genetic correlation analysis, strongly support a functional model linking Slt2 MAP kinase and Pcl1, a Pho85 cyclin-dependent kinase, in septum assembly through Bni4. This model, based on the coordinated phosphorylation of Bni4 by both kinases, would be able to integrate cellular signals rapidly to maintain cell integrity during cytokinesis.

To whom correspondence should be addressed: César Roncero, IBFG and Departamento de Microbiología and Genética, IBFG C/ Zacarías Gonzalez nº1, 37007, Salamanca, Spain. crm@usal.es.

INTRODUCTION

In yeast, cytokinesis is the final step of a well orchestrated process in which contraction of the actomyosin ring (AMR) is coupled to the synthesis of a primary septum that physically separates mother and daughter cells. Cytokinesis is triggered definitively by the activation of the Mitotic Exit Network (MEN) cascade, which allows the recruitment of AMR to the neck constriction (for a review, see Roncero and Sanchez 2010). However, the assembly of the machinery directing this process occurs well before, and one of the initial steps in this process is the assembly of the septin ring, a very conspicuous structure localized at the bud neck, along the cell division process. The septin ring acts as a scaffold, directing the assembly of other components of the septum machinery, including the AMR, at the time of cytokinesis. Based on this, it is not surprising that the septin ring is an essential structure that has been under extensive scientific scrutiny for many years in different organisms (for recent reviews, see Fung *et al.* 2014; Oh and Bi 2011). Among the multiple functions described for the septins, here we focus on its function as a scaffold for Bni4 (DeMarini *et al.* 1997), which in turn recruits the phosphatase Glc7 and the chitin synthase III regulator Chs4 to the neck (Kozubowski *et al.* 2003). Bni4 interacts physically with Chs4 (DeMarini *et al.* 1997), which is the only known Chitin Synthase III (CSIII) activator, and hence Bni4 contributes directly to the proper localization of active CSIII at the neck and to the correct assembly of the chitin ring (Larson *et al.* 2008; Sanz *et al.* 2004). To date it is unclear whether Bni4 might perform additional functions in CSIII regulation. What has become clear over the years is that Bni4 must perform functions at the neck other than regulating CSIII (Larson *et al.* 2010). However, these functions do not seem to be essential since they have only been detected in hypersensitized yeast strains. These studies suggested a minor role for Bni4 in the proper assembly of the septin ring, a role that has so far been linked to the phosphorylation of Bni4 by Pho85 G1 Cyclin-dependent kinases (Zou *et al.* 2009). This phosphorylation regulates the intracellular localization of Bni4, contributing to the coordination between the cell cycle and septum assembly (Larson *et al.* 2010; Zou *et al.* 2009); however, other kinases have also been proposed to contribute to Bni4 phosphorylation. Thus, despite the extensive studies already carried out the precise function of Bni4 at the neck remains poorly defined.

In *S.cerevisiae* the chitin ring accounts for approximately 90% of total cellular chitin but is not essential, and its functional relevance only became apparent after SGA analyses (Lesage *et al.* 2005). Later, the chitin ring was shown to play a homeostatic role in the maintenance of cell integrity at the time of cytokinesis (Cabib and Schmidt 2003; Gomez *et al.* 2009), which would explain the complex pattern of synthetic lethality associated with the absence of CSIII activity. In addition, CSIII is also involved in the cellular response to cell wall damage, a response directly mediated by the Cell Wall Integrity (CWI) cascade. The activation of this response triggers the phosphorylation of the transcription factor Rlm1 by the MAP kinase Slt2 and a

massive transcriptional response that includes the up-regulation of CSIII activity (for a review, see (Levin 2011). This transcriptional response is not unique, since CWI also acts on the SBF (Swi4/6 cell cycle box binding factor) complex in order to coordinate the cell cycle and cell wall synthesis (Madden *et al.* 1997). Moreover, several lines of evidence point to additional roles for the individual components of the CWI, which could include the phosphorylation of additional non-nuclear targets. In this regard, it is worth noting that Slt2 localizes to the sites of polarized growth (van Drogen and Peter 2002), although its function at these sites remains unexplored.

Previous work from our laboratory reported the synthetic lethality (SL) of the double *slt2*Δ *rim101*Δ mutant promoted by the concomitant absence of CWI and RIM101 signaling transduction pathways (Castrejon *et al.* 2006). This lethality turned to be independent of the transcriptional response mediated by the CWI and was linked to a incorrect synthesis of the septum caused by the absence of Slt2 kinase, aggravated by the upregulation of the Cts1 chitinase activity caused by the *rim101*Δ mutation (Gomez *et al.* 2009). Interestingly, these defects were also associated with an altered localization of Bni4 at the neck in the *slt2*Δ mutant. The synthetic lethality was reversed by overexpression of the *GFA1* or *CCT7* genes, which reinforced septum architecture through independent mechanisms (Gomez *et al.* 2009). These results, together with previous evidence, suggest a yet undefined role for Slt2 in septum assembly, a role that could potentially be linked to the phosphorylation of Bni4.

Our extended search for the suppression of the synthetic lethality of the *slt2*Δ *rim101*Δ mutant yielded the *PCL1*, *KSS1* and *SPH1* genes as multicopy suppressors, highlighting a potential role of multiple kinases in septum assembly. Detailed characterization of the suppression by the MAP kinase Kss1 revealed that either Slt2 or Kss1 mediates Bni4 phosphorylation, contributing to the proper assembly of the septum. Therefore, coordinated phosphorylation of Bni4 by multiple kinases would constitute an additional level of coordination in septum assembly during the cell cycle.

EXPERIMENTAL PROCEDURES

Strains, Plasmids and Yeast Genetics Methods. Standard procedures were employed for yeast genetics (Rose *et al.* 1990) and DNA manipulations (Sambrook *et al.* 1989). The *S.cerevisiae* strains used in this study and their sources are listed in Table 1. Single mutants were made using the one-step gene replacement technique. The plasmids used throughout this work are listed in Table 1 and most of them have been described previously. Kss1 protein was tagged at its C-terminus with 1xGFP on the genome or on the plasmid pRS426*::KSS1,* employing an integrative cassette amplified from pFA6a-GFP-hphMx6 plasmid. Bona fide plasmids expressing *Kss1-GFP* were later recovered in *E.coli* and sequenced. For the construction of pRS314::*BNI4-YFP* the yellow fluorescent protein (YFP) tag was introduced as a NotI fragment

at a NotI site created specifically at the last codon of *BNI4*, following a strategy previously used in our laboratory (Cos *et al.* 1998). The tagged protein was confirmed to be functional in the *bni4*Δ mutant. Non-phosphorylatable versions of Bni4 were made by site-directed mutagenesis, as described (Kunkel *et al.* 1987), using this plasmid as template. Bni4-YFP localization (see below) was routinely tested in strains containing the wild-type Bni4 protein, but the functionality of the mutated forms of Bni4 was always tested in *bni4*Δ strains.

Media and growth conditions. YEPD (1% yeast extract, 2% peptone, and 2% glucose) or synthetic minimal medium (SD) (0.7% yeast nitrogen base without amino acids and 2% glucose) supplemented with appropriate amino acids and nucleic acid bases were routinely used as media. Cell cultures were typically obtained by diluting an O/N culture grown on YEPD or selective SD (when required) in fresh media up to an OD_{600} of 0.2 (~ 3.5 x 10^6 cells/ml) and further growth for 2 generation times prior to collection. Cell wall stress was produced by treating exponential cultures grown at 28ºC on YEPD with 0.075 mg/ml of calcofluor, 3mM caffeine or 5 U/ml of Zymolyase for 1 hr. α-factor treatment was performed using it at 10μg/ml concentration for 1 hour. Alternatively, plain YEPD or SD with or without 15 mM glucosamine, 2.5 mM caffeine or 100 ng/ml caspofungin was used in some of the experiments, as indicated. For the growth of synthetic lethal mutants, the media were routinely supplemented with 1M sorbitol. Growth of the different mutants was assessed in YEPD media, but SD medium was used in all experiments involving plasmid-containing cells.

Microscopy techniques. Calcofluor vital staining was observed in cells grown in YEPD (±1M Sorbitol) in the presence of 50μg/ml calcofluor for 2 h at 28°C. Alternatively, the chitin ring was observed in fixed cells (3.2% formaldehyde, 30min) stained with calcofluor for 5 min (Arcones and Roncero 2016; Gomez *et al.* 2009). For YFP/GFP visualization, yeast cells containing the corresponding centromeric plasmid were grown to early logarithmic phase in selective SD (±1M Sorbitol) medium supplemented with 0.2% adenine. All microscopy observations were performed with a Nikon 90i epifluorescence microscope with a 100W Hg lamp, using the appropriate filters (Chroma 49000 ET-DAPI, 49002 ET-GFP or 49003-ET-YFP) and a 100xCFI Plan Apochromat (n.a. 1.45, oil) objective. Images were obtained with an ORCA ER camera using the MetaMorph sowftware (V-7.5.6.0) and processed with Adobe Photoshop CS5 software. All images shown in each figure were acquired under identical conditions and processed in parallel to preserve the relative intensities of fluorescence for comparative purposes. Cell measurements are expressed in micrometers (μM) and are the average values from more than 50 cells (n>50). They were performed on digital images using the tools included in the ImageJ software (NIH). * indicates values significantly different from the wild-type ($p<0.05$).

Zymolyase sensitivity assays. Yeast sensitivity to Zymolyase was assayed as growth inhibition ratios, as described previously (Gomez *et al.* 2009). Briefly, cells were pre grown, diluted to an OD600 of 0.005, and further incubated for 24 h at 28°C in YEPD or 1 M sorbitol-supplemented YEPD in the presence of different Zymolyase 100T (Seikagaku Corp.) concentrations. Growth was then determined by measurement of the OD_{600} of each culture. The data are expressed as the percentage of growth relative to the cultures grown without Zymolyase.

Immunoblot analyses. Typically, proteins were analyzed by Western blotting after sodium dodecyl sulfate-polyacrylamide gel electrophoresis and immunoblotting as described previously (Pérez *et al.* 2010), but increasing the transference time to 2h. To detected minor relative differences in migration, the acrylamide percentage was adjusted as indicated. Alternatively, proteins were separated on 3-8% continuous gradient SDS–PAGE gels (Biorad) or using 100 mM Mn^{+2}- Phos-tag^{tm}Acrylamide AAL-107 (NARD institute, ltd.) in SDS-PAGE gels following the manufacturer's instructions. In the latter case, total protein extracts were prepared using the trichloroacetic acid (TCA) protein extraction protocol (Foiani *et al.* 1994). The commercial mouse monoclonal antibodies anti-HA (12CA5, Roche Diagnostics; 1:4000 dilution) and the anti-GFP (JL-8, Clontech Laboratories, Inc 1:1000 dilution) were used to detect HA or GFP/YFP epitope-fused protein on immunoblots. The phosphorylated forms of the MAPK kinases Slt2, Fus3 and Kss1 were detected by immunoblot as described (Pérez *et al.* 2010), using anti-phospho-p42/44 antibody (Phospho-p44/42 MAPK Antibody #9101, Cell Signaling Tecnology, Inc) at 1:2500 dilution.

Immunoprecipitation and alkaline phosphatase assays. For the immunoprecipitation of the Bni4-YFP fusion protein, cells from 100 ml of logarithmically growing cultures were harvested by centrifugation and washed once in the same volume with cold 10 mM Tris-HCL pH7. Cells were lysed, as described above, in 800 - 1000 µl of immunoprecipitation lysis buffer (IPB) (50 mM Tris-HCl, pH 7.0, 0.1% Triton, 150 mM NaCl) containing protease inhibitor cocktail (2 mM PMSF, 5 mM EDTA, 5 mM EGTA and 2 µg/ml each of leupeptin, pepstatin A and aprotinin) and phosphatase inhibitor cocktail (10 mM sodium pyrophosphate, 1 mM sodium orthovanadate). The lysates were cleared of cell debris (5 min, 16000g, 4°C). Approximately, 600 - 700 micrograms of total protein from cell lysates was brought up to 300µl with IPB buffer. In order to avoid unspecific interactions, this suspension was mixed with 50µl of 0.1 mg/ml of Protein A-Sepharose (GE Healthcare) diluted in IPB, and incubated for 1 hr at 4ºC in a rotating device. Then, this suspension was centrifuged (4 min, 1500g) and the supernatant was recovered. The cleared suspension was incubated with the rabbit polyclonal anti GFP antibody (A-6455, Invitrogen) at 1:100 dilution at 4°C for 2 h, and then mixed with 50µl of 0.1 mg/ml of

Protein A Sepharose and incubated for a further 2 h**.** The resin was washed three times with IPB and boiled with 50 µl of 4× SDS loading buffer for 5 min. Samples were separated on SDS-PAGE gels and visualized by immunoblotting, as indicated above.

Phosphatase assays on Bni4-YFP protein were performed as described previously (Kozubowski *et al.* 2003) with minor modifications. After immunoprecipitation, the resin was washed 4 times using phosphatase buffer containing 2mM PMSF (PB) and finally resuspended in 100µl of PB. The reaction using calf intestinal alkaline phosphatase (Roche Diagnostics) was carried out at 37ºC for 30 min. This protocol was technically incompatible with the use of Phos-tag^{tm}Acrylamide gels and the proteins were always resolved in regular SDS-PAGE gels and visualized by immunoblotting, as indicated above.

Co-immunoprecipitation assays. Bni4-3xHA and Slt2-GFP-tagged proteins were used to determine protein-protein interactions in co-immunoprecipitation assays as follows: Slt2-GFP was immunoprecipitated exactly as described above using rabbit polyclonal anti GFP antibody (A-6455, Invitrogen) at 1:100 dilution. The resulting immunoprecipitate was divided into two aliquots, separated in SDS-PAGE gels and later developed by immunoblotting using either anti-GFP or anti-HA antibodies as described above in order to visualize Slt2-GFP and Bni4-3xHA respectively. Alternatively, Bni4-3xHA protein was immunoprecipitated using the polyclonal anti-HA antibody (Ha.11, Covance) using a similar protocol.

The co-immunoprepipitatiom assays for determining Bni4 and Kss1 interaction were performed in cells containing plasmids pRS314*::BNI4-3xHA* and pRS426*::KSS1-GFP*. Proteins extracts were obtained as above and samples were diluted with IPB to a final protein concentration of 0,8 mg/ml. We next incubated 1 ml of the protein sample with 50µl of Anti-GFP MicroBeads (Miltenyibiotec) and 2% BSA for 30 min at 4ºC in an orbital rotator. After that, mixtures were applied onto µColumns placed in the µMACS^{TM} Separator and washed with the different buffers following instructions provided by the kit. Proteins bounded specifically to Anti-GFP MicroBeads were eluted with 50µl of pre-heated 95ºC elution buffer applied directly to the column. Finally, all samples were boiled for 5 min, and then separated in SDS-PAGE gels visualized by immunoblotting.

β-Galactosidase Assays. β-Galactosidase assays were performed in a strain containing the *MLP1-LacZ* transcriptional reporter fusion (García *et al.* 2009). Protein extracts were obtained from 30ml of mid-log cultures, as described previously (Rose *et al.* 1990) using a 2mM PMSF final concentration in sample preparation. β-galactosidase activity was expressed as nanomoles of *o*-nitrophenyl-β-D-galactopyranoside (ONPG) converted per minute per milligram of protein.

Measurements were preformed by duplicated and values presented are the average of three independent experiments.

RESULTS

KSS1 overexpression suppresses the defects in septum assembly of the slt2Δ rim101Δ mutant. We have previously shown that the synthetic lethality of the *slt2*Δ *rim101*Δ mutant can be suppressed by overexpression of the *GFA1* or *CCT7* genes, both acting through independent mechanisms in the reinforcement of the damaged architecture at the yeast neck (Gomez *et al.* 2009). However, our suppression screening also revealed additional suppressor genes, namely *PCL1*, *SPH1* and *KSS1*, all of them able to sustain the growth of the *slt2*Δ *rim101*Δ mutant in non-osmotically stabilized media (Figure 1A). Interestingly, the three suppressor genes encode proteins putatively linked to Slt2 function. *PCL1* overexpression has been shown to suppress the *slt2*Δ mutant, a suppression linked to the role of the SBF transcription factor in cell cycle regulation (Baetz *et al.* 2001; Madden *et al.* 1997). Sph1 is a close homologue of Spa2, both acting as scaffolds for the tethering of the Slt2 kinase module to the sites of polarized growth (Roemer *et al.* 1998; van Drogen and Peter 2002). Finally, Kss1, like Slt2, is one of the MAP kinases identified in yeasts and it has been linked physiologically to Slt2 through the SVG (Ste Vegetative Growth) pathway (Lee and Elion 1999), although their relationship remains obscure. This indirect evidence, together with the overall results of our suppression screening, suggested a potential role for Kss1 kinase in neck architecture, a role that could potentially highlight the poorly described role of Slt2 kinase in septum assembly (Tahirovic *et al.* 2003).

In order to explore the possible connection between these suppressors we first characterized the suppression exerted by Kss1 on the *slt12*Δ *rim101*Δ mutant. The overexpression of *KSS1* in either the original YEp13 vector or in the multicopy pRS424 plasmid significantly improved the growth of the mutant in the absence of osmotic support (Figure 1A). The suppression did not increase chitin synthesis as assessed by calcofluor staining (Fig 1B), but restored Bni4 wild-type localization by increasing the number of double rings of Bni4 at the neck (Fig 1C). Similar results were obtained when the other suppressor, PCL1, was overexpressed (not shown). This suppression was somewhat different from that observed for *GFA1* overexpression (Figure 1B) but similar to that of *CCT7* (not shown, see (Gomez *et al.* 2009)), suggesting the involvement of Kss1 and Pcl1 kinases in septum assembly rather than in chitin up-regulation, similarly to what has been previously proposed for Slt2 (Tahirovic *et al.* 2003).

KSS1 partially suppresses slt2Δ phenotypes independently of transcriptional activation. Work with the synthetic lethal s*lt2*Δ *rim101*Δ mutant requires the continuous maintenance of osmotic support, and the results obtained are thus difficult to interpret. Accordingly, we wondered

whether *KSS1* overexpression might be able to suppress the phenotypes classically associated with the single *slt2*Δ mutant, which is able to grow normally at 28 ºC. The *slt2*Δ single mutant grew poorly in the presence of 2.5mM caffeine and at 38ºC (Figure 2A), and the overexpression of *KSS1* clearly improved its growth in 2.5 mM caffeine, but not at 38ºC. In contrast, chitin synthesis upregulation associated to *GFA1* overexpression improved growth significantly under both conditions. Overexpression of *KSS1* from the *GAL1* promoter produced similar results, being still unable to restore growth of the *slt2*Δ mutant at 37ºC. In addition, overexpression of the catalytically inactive Kss1^{K42R} mutant (Madhani *et al.* 1997) did not suppress caffeine hypersensitivity, suggesting that suppression is directly dependent on the function of Kss1 as a protein kinase. Moreover, the suppression observed seemed to be specific for this protein kinase since the overexpression of other related MAP kinases, such as Fus3 or Hog1 (Chen and Thorner 2007), was not able to improve the growth of the *slt2*Δ mutant under caffeine treatment (Figure 2A).

We next explored other phenotypes associated with the *slt2*Δ mutation. The *slt2*Δ mutant is extremely sensitive to Zymolyase (Figure 2B), and overexpression of *KSS1* alleviated such sensitivity only to a moderate extent. Interestingly, *GFA1* overexpression restored zymolyase resistance to wild-type levels, indicating that *GFA1* acts as a better suppressor of the *slt2*Δ mutant phenotype than *KSS1* under all conditions tested. In order to test a potential effect of the higher levels of Kss1 kinase through the CWI pathway, we addressed the effect of *KSS1* overexpression directly on the CWI response by measuring the expression levels of the *MLP1-LacZ* reporter (Figure 2D, (García *et al.* 2009). *KSS1* overexpression produced a moderate increase in β-galactosidase levels in the wild-type strain either under normal growth or after cell wall damage induced by Zymolyase or calcofluor treatment, both of which induced the CWI response, leading to a significant increase in the levels of the *MLP1-LacZ* transcriptional reporter. This increase is probably an indirect effect of Kss1 overexpression on the levels phosphatases known to negatively regulate the CWI signaling (Sacristán-Reviriego *et al.* 2015). However, and much more importantly, *KSS1* overexpression failed to restore β-galactosidase levels in the *slt2*Δ mutant, which showed a complete blockade of the CWI transcriptional response triggered by Zymolyase or calcofluor. It may therefore be concluded that higher levels of Kss1 suppresses *slt2*Δ phenotypes independently of the transcriptional role played by Slt2 in the CWI response.

We also tested the localization of Bni4, which in our experimental conditions was characterized by a high proportion of double rings at the neck, a proportion that was significantly reduced in the *slt2*Δ mutant (Figure 2C, and (Gomez *et al.* 2009). Overexpression of *KSS1* restored the number of double rings to wild-type levels, pointing to a specific role for Kss1 overexpression in the septum machinery.

Altogether the results obtained highlight the existence of alternative targets for Slt2 outside its transcriptional effectors that could be shared with Kss1 based on the characteristics of the suppression observed.

Slt2 and Kss1 MAPK kinases act redundantly in controlling septum assembly. Kss1 forms part of the mating and invasive growth signaling pathways in yeast, and its role in the transcriptional response of these routes has been described extensively (Schwartz and Madhani 2004). In addition, Kss1 has also been reported to be part of the SVG response, which triggers an alternative response after cell wall damage. This response would overlap the CWI response functionally, although the nature of this overlap is only partial and somewhat unclear (Lee and Elion 1999). To date, there is no experimental evidence about any role of Kss1 during vegetative growth that might account for the suppression of the *slt2*Δ mutant phenotypes, including localization of the protein at the neck. Therefore we first determined Kss1 intracellular localization by fluorescence microscopy. Accordingly to previous reports (http://images.yeastrc.org/imagerepo/searchImageRepoInit.do), Kss1-GFP localized mostly at the nucleus of vegetative cells being barely visible at the neck; however, after overexpression Kss1-GFP could be neatly localized at the neck (Figure 3A), thus being able to act at this cellular localization. Next we also compared the individual phenotypes of *kss1*Δ with those of *slt2*Δ (Figure 3). The *kss1*Δ mutant did not show significant hypersensitivity to caspofungin or caffeine, two of the characteristic traits of the *slt2*Δ mutant (Fig 3B). In contrast, *kss1*Δ showed partial growth at low concentrations of calcofluor, although the *kss1*Δ mutant apparently had normal calcofluor staining and chitin rings at the neck (Figure 3C, see also below). The Bni4 localization at the neck of *kss1*Δ was also similar to the controls (Figure 3D), in contrast to the phenotype observed in the *slt2*Δ mutant, which showed significantly reduced numbers of Bni4-YFP double rings at the neck (Figure 2C). Moreover, activation of the CWI response occurred normally in the *kss1*Δ mutant after calcofluor (Figure 3E) or caffeine treatment (not shown). In addition, the absence of Slt2 did not seem to trigger the phosphorylation of Kss1 or Fus3 kinases. All these observations clearly indicate that the *kss1*Δ mutant did not share the defects classically associated with the absence of Slt2, the MAP Kinase of the CWI pathway.

We next tested the functional overlap of Kss1 and Slt2 kinases by characterizing the *kss1*Δ *slt2*Δ double mutant. This mutant was isolated in medium containing 1M sorbitol and displayed apparently normal growth in osmotic stabilized media. However, it did not grow in plain YEPD or Complete SD medium (Figure 4A and data not shown). This failure to grow was associated with a high degree of lysis upon transferring the cultures from osmotic supplement media to plain media (Figure 4B, and data not shown). The poor growth of the double mutant was associated with the presence of abnormal neck structures (Figure 4B, arrow heads). Interestingly, supplementation of the media with N-Acetyl glucosamine restored normal growth

(Figure 4A) by preventing cell lysis (not shown), suggesting that the effects of the absence of Slt2 and Kss1 kinases can be alleviated again by the upregulation of chitin synthesis (Bulik *et al.* 2003; Gomez *et al.* 2009). It has been shown that proper septum assembly depends on the chitin ring (Gomez *et al.* 2009; Schmidt *et al.* 2003) and, intriguingly, when incubated in osmotically supplemented media the *slt2*Δ *kss1*Δ mutant showed significantly wider chitin rings than those observed in the wild-type or single mutant cells (Figure 4C, D). This alteration was also associated in the double mutant to wider rings of the Bni4-YFP or Cdc3-GFP proteins (Figure 4C). Moreover, vital calcofluor staining revealed a significant enlargement of the bud and birth-scar region, rendering the bud scars very prominent (Figure 4E); this phenotype was not observed in either *slt2*Δ (Figure 4E) or *kss1*Δ individual mutants. These aberrant neck structures would be prone to lysis upon cell transfer to plain medium, explaining the high degree of lysis and poor growth of this *kss1*Δ *slt2*Δ mutant in non-osmotically stabilized media. Together, the above findings point to severe problems in septum assembly in the double mutant. In sum, although the phenotypes observed for the *kss1*Δ mutant do not correspond to those associated with the absence of the CWI pathway, Kss1 seems to act in the assembly of the yeast cell wall septum during cytokinesis, at least when the function of Slt2 is compromised.

Bni4 is a potential substrate for Slt2 and Kss1 MAP kinases. The results reported above thus pointed to common targets for Slt2 and Kss1 kinases at the yeast neck, where both have been shown to localize partially (Figure 3A and Roemer *et al.* 1998; van Drogen and Peter 2002). Such a target has been proposed to exist for Slt2 previously, but this has never been confirmed experimentally (Levin 2011). Moreover, our results point to Bni4 protein as a putative target for these kinases, since the absence of Slt2 triggered a Bni4 delocalization, alleviated by Kss1 overexpression (Figure 2C). Bni4 has previously been shown to be phosphorylated, this phosphorylation being important for its biological function (Kozubowski *et al.* 2003; Zou *et al.* 2009). Accordingly, we tested Bni4 phosphorylation in the *slt2*Δ mutant. Bni4 is a 100-kDa protein that typically runs with an apparent molecular weight close to 200 kDa when tagged with the YFP in a wild-type strain (Figure 5A and Kozubowski *et al.* 2003)). Interestingly, Bni4-YFP showed a small but consistently higher mobility in the *slt2*Δ mutant (Figure 5A). The use of Phos-tag gels increased the differences in mobility for Bni4 between the wild-type and *slt2*Δ strains (Fig 5A, see lower panel), suggesting that these differences would be due to changes in the phosphorylation status of Bni4 in the *slt2*Δ mutant, and pointing to Bni4 as a substrate for Slt2 kinase. However, Bni4-YFP obtained from the *slt2*Δ mutant still increased its mobility after alkaline phosphatase (AP) treatment (Figure 5B), indicating that Bni4 remained partially phosphorylated in the absence of Slt2 kinase, a clear indication for the phosphorylation of Bni4 by several protein kinases, in agreement with previous reports (Zou *et al.* 2009). In order to test whether Kss1 kinase contributed to Bni4 phosphorylation we tested the effect of the

overexpression of *KSS1* on Bni4. This overexpression reduced the mobility of the Bni4 protein in both the wild-type (Figure 5C, left panel) and the *slt2*Δ strains (Figure 5C, right panel). Moreover, Bni4 mobility after *KSS1* overexpression was restored to wild-type levels after AP treatment, indicating that its reduced mobility was due directly to the increased phosphorylation caused by *KSS1* overexpression.

However, this evidence is not a probe of a direct relationship between these MAP kinases and Bni4 since the changes on its phosphorylation levels could have been an indirect effect of the role of these kinases. We therefore first addressed the physical interaction between Slt2 and Bni4 proteins in co-immunoprecipitation (IP) assays (Figure 5D). Slt2-GFP was immunoprecipitated using an anti-GFP polyclonal antibody, and the immunoprecipitate was developed with anti-HA to detect the Bni4-3xHA protein. Only in protein extracts obtained from wild type strain co-expressing Slt2-GFP and Bni4-3xHA were we able to detect a discrete band that was reactive to the anti-HA monoclonal antibody that would correspond in size to the Bni4-3xHA protein (lane 3). This band did not appear in the absence of Slt2-GFP (lane 1), indicating a physical association between the Slt2 and Bni4 proteins. A more detailed analysis of this interaction in two-hybrid assays was not technically possible owing to the higher background afforded by the fusions of Slt2 (data not shown) due to its intrinsic binding to DNA (Kim *et al.* 2007). Next, we also addressed the direct interaction between Bni4 and Kss1 proteins by co-immunoprecipitation. As shown in Figure 5E, immunoprecipitation of Kss1-GFP pulled down specifically Bni4-3xHA, a clear indication of the physical interaction between both proteins, previously anticipated by PCA analysis (Hruby *et al.* 2011).

Altogether, these results indicated that Bni4 interacts physically with both Slt2 and Kss1. Therefore; Bni4 could be a direct substrate for both MAPK kinases, explaining how the absence of Slt2 could lead to a reduced phosphorylation of Bni4 that can be reversed by the overexpression of the related Kss1 kinase.

MAP Kinase phosphorylation sites in Bni4 are required for its proper function. In order to find support for the hypothesis of a possible phosphorylation of Bni4 by MAPK kinases such as Slt2 or Kss1, we searched for MAP kinase phosphorylation sites that could be associated with the changes in phenotypic expression of Bni4-YFP described in this work. Bioinformatics analysis indicated that Bni4 contains 38 potential phosphorylation sites, 11 of which are potential MAPK substrate sites (KinasePhos, 100% specificity). We focused our work on the 5 potential MAPK sites indicated in Figure 6A because residues S364, T689 and T769 were shown to be phosphorylated *in vivo* (Albuquerque *et al.* 2008; Chi *et al.* 2007), http://www.phosphogrid.org/sites/35605/YNL233W.phospho), while residues T427 and T443 are part of the consensus TPL site phosphorylated by Slt2 in the transcription factor Rlm1 (Jung *et al.* 2002). In order to create non-phosphorylatable residues, we successfully replaced the 364,

427, 443 and 769 S/T residues by alanine, but failed to obtain the T689A mutant. Following this, we introduced the four individual non-phosphorylatable mutants created in *bni4*Δ yeast cells, and the localization of the corresponding proteins was assessed by fluorescence microscopy. As shown in Figure 6B, the Bni4^{S364A}-YFP, Bni4^{T443A}-YFP and Bni4^{T769A}-YFP proteins showed identical localization to Bni4-YPF, but cells containing the Bni4^{T427A}-YFP protein showed a significantly reduced number of double rings at the neck ($p < 0.05$); this localization pattern that resembled that observed in the *slt2*Δ mutant (Figure 2C). However, all these cells containing the mutated versions of Bni4 showed normal patterns of calcofluor staining and wild type levels of resistance to this drug (data not shown), making the potential phenotypes of these mutants difficult to follow experimentally. We therefore searched for a hypersensitive assay that could help us in the identification of additional phenotypes for these Bni4 non-phosphorylatable mutants.

We have previously shown that the absence of Bni4 increases the thermosensitivity of the *cdc10-11* mutant (Figure 6C, (Sanz *et al.* 2004), rendering the double mutant *cdc10-11bni4*Δ unable to grow at 32ºC. We therefore transformed this double mutant with the different versions of Bni4 made and assessed their growth at 32 ºC. Wild-type Bni4-YFP and Bni4^{S769A}-YFP restored growth at 32 ºC to levels similar to the single *cdc10-11* mutant. However, the Bni4^{S364A}-YFP, Bni4^{T427A}-YFP and Bni4^{T443A}-YFP proteins failed to support growth at 32 ºC, suggesting that Bni4 function would be impaired in these cells due to the absence of these phosphorylation sites, thereby highlighting the importance of phosphorylation in Bni4 function.

Above, we reported that overexpression of the MAP kinase *Kss1* suppresses *slt2*Δ phenotypes (Figure 2), likely by increasing Bni4 phosphorylation (Figure 5C). If this hypothesis were true, then *KSS1* overexpression should also suppress the strong thermosensitive phenotype of the *cdc10-11slt2*Δ double mutant (Figure 6D), and this was indeed the case since this overexpression alleviated the slow growth of this mutant at 28 ºC, restoring partial growth even at 32 ºC (Figure 6D). The model also predicts that high levels of Kss1 kinase would not have effect in the absence of Bni4 and, accordingly, *KSS1* overexpression did not improve the growth of the double *cdc10-11bni4*Δ mutant at 32ºC. The next question to be addressed was the relative importance of the phosphorylatable sites of Bni4 described above on Kss1 suppression. We therefore overexpressed *KSS1* in *bni4*Δ *cdc10-11* cells containing the different non-phosphorylatable Bni4 mutants (Figure 6E). High levels of the Kss1 kinase partially restored growth at 32 ºC in the strains containing the Bni4^{S364A}-YFP and Bni4^{T443A}-YFP proteins, but not the Bni4^{T427A}-YFP mutant. However, the growth of these two mutants at 32ºC was significantly slower than that observed for the cells containing the wild-type Bni4, indicating only partial suppression. Together, these results clearly indicate that the T427 phosphorylatable residue of Bni4 is critical for the function of the protein in the *cdc10-11* background, while the absence of S364 or T443 phosphorylatable residues can be partially compensated by *KSS1* overexpression,

probably via the phosphorylation of Bni4 at additional residues. Interestingly, the overexpression of *KSS1* also improved the growth at 32 ºC of different *cdc10-11* strains (compare images in Figures 6C, D and E), highlighting a functional role of Kss1 in septum assembly when overexpressed.

DISCUSSION

The identification of new suppressors for the lethal synthetic phenotype of the *rim101*Δ *slt2*Δ has provided additional evidence for our understanding of the role of Slt2 kinase in the correct assembly of yeast septa. The identification of two kinases as suppressors was not unexpected, owing to the biochemical redundancy between different kinases, but our results clearly favor a model based on the action of these suppressor kinases, Pcl1 and Kss1, on common targets. This is especially clear in the case of the MAP kinase Kss1, whose suppression depends on its kinase activity and cannot be exerted by the related MAP kinases Hog1 or Fus3. Moreover, both Kss1 and Slt2 can be localized at the neck (Figure 3A and van Drogen and Peter 2002), respectively). Interestingly, our screening also identified Sph1 as week multicopy suppressor (Figure 1A), a protein described as a scaffold for the components of the CWI and STE signaling pathways at the site of polarized growth (Roemer *et al.* 1998), pathways in which the MAP kinases Slt2 and Kss1 form part respectively. High levels of Sph1 could therefore increase the accumulation of Kss1 at defined sites, explaining the observed suppression. This localization effect would be consistent with the existence of targets for the MAP kinases Slt2 and Kss1 at the sites of polarized growth, a hypothesis held over the years for Slt2 (Levin 2011; Li *et al.* 2013) but unsupported by solid experimental evidence.

Our results not only support this hypothesis but also place these targets within the machinery involved in the synthesis of cell wall at the septum because to the additive phenotypes observed in the strain simultaneously lacking the Slt2 and Kss1 kinases. Accordingly, upregulation of chitin synthesis by glucosamine addition or *GFA1* overexpression, alleviated these phenotypes in agreement with the homeostatic role proposed for the chitin ring during cytokinesis (Gomez *et al.* 2009; Schmidt *et al.* 2003). The results presents here point to Bni4 as potential substrate at the neck for both kinases, because it was under-phosphorylated in the *slt2*Δ mutant and the overexpression of Kss1 led to hyper-phosphorylated forms of Bni4. Moreover, the co-immunoprecipitation observed between Bni4 and both kinases (Figure 5D,E), together with the physical interaction reported between Kss1 and Bni4 (Hruby *et al.* 2011), place Bni4 as a direct substrate for either of these kinases, which would be in agreement with a redundant role of both kinases. However, the function of these kinases in cell integrity must exceed that of the phosphorylation of Bni4 since the *bni4*Δ mutant is not lethal and only showed mild morphogenetic phenotypes (DeMarini *et al.* 1997; Kozubowski *et al.* 2003; Sanz *et al.* 2004;

Zou *et al.* 2009). The role of Slt2 as part of the CWI response (Levin 2011) is clear, but the phenotypes of Kss1 during vegetative are minor, and only highlighted in the presence of additional mutations (see Figure 4 and Lee and Elion 1999). Moreover, only high levels of Kss1 were able to alleviate partially the absence of Slt2. Such functional levels could be obtained by increasing Kss1 levels directly or, to a lesser extent, by increasing the levels of the Sph1 scaffold, which would explain its suppressor action. Altogether, the results reported suggested that while Bni4 would be a bona fide target for Kss1, other targets of Kss1 should exist at the neck. Surprisingly, we failed to identify the Sph1 paralog Spa2 as a suppressor in our screening, probably owing to the higher affinity of Spa2 for the proteins involved in Slt2 activation (Sheu *et al.* 2000) and the different biological role reported for Spa2 or Sph1 in vegetative growth (Li *et al.* 2013).

Regardless of the higher relevance of Slt2 in septum assembly, the function of both kinases seems to be at least partially exerted through Bni4 phosphorylation, since some of the Bni4 phosphorylation mutants encompassed the phenotypes associated with the absence of Slt2, such as the reduced number of double Bni4 rings (Bni4^{T427A}) or the increased thermosensitivity in the *cdc10-11* background (Bni4 ^{S364A}, Bni4 ^{T427A} or Bni4 ^{T443A}). Moreover, the suppression by *KSS1* depends not only in the presence of Bni4, but also on the presence of defined phosphorylatable sites in this protein. Residues S364, T427 and T443 are required for proper the functioning of Bni4 in the *cdc10-11* background, but, interestingly, only the absence of the S364 and T443 phosphorylatable residues could be partially compensated by the protein kinase activity of Kss1 expressed at high levels, suggesting that phosphorylation at T427 could be essential for proper Bni4 function, at least in our sensitization assays.

Bni4 function has also been shown to be dependent on phosphorylation by Pcl1/2 Pho85 cyclin-dependent kinases, although only one multiple mutant lacking 10 S/T phosphorylation sites, which included the T427 mutation, has biological phenotypes (Zou *et al.* 2009). Here we also identified *PCL1* as suppressor of the SL of the *slt2*Δ *rim101*Δ mutant, and it is therefore tempting to speculate about the possibility of the T427 site being a target for the Pcl1 kinase, as suggested (Zou *et al.* 2009). Upon overexpression, this kinase would phosphorylate T427 in the absence of Slt2, leading to the observed suppression. Such a redundancy in phosphorylating Bni4 is fully compatible with evidence indicating that neither Pcl1/2 (Zou *et al.* 2009) nor Slt2 (this work) could account for the complete phosphorylation of Bni4. Our results thus uncover an additional level of cross talk between the regulatory mechanisms mediated by the Slt2 and Pcl1 kinases, beyond the previously reported linkage through the SBF cell cycle regulator (Madden *et al.* 1997).

An intriguing question regarding the present work and others is the specific function of Slt2 at the sites of polarized work, a function that has remained masked due to the strong transcriptional response triggered by this MAP kinase as part of the CWI response. Recently

Slt2 has been shown to regulate ER cortical inheritance, probably by phosphorylating a yet undefined substrate at the tip of the bud (Li *et al.* 2013). However, this function is unlikely to be related to Bni4 since this protein localizes to the neck and the *bni4*Δ mutant did not show any apparent defect in the cortical inheritance of the ER (not shown). Our work clearly links the action of Slt2 at the neck to Bni4 function, but unfortunately the precise role of this protein remains uncertain. Bni4 participates in the assembly of the chitin ring, contributing to the localization of Chs3/4 at the neck (DeMarini *et al.* 1997; Kozubowski *et al.* 2003; Sanz *et al.* 2004) but, based on assays using hypersensitized cells, it is also suspected to contribute to septin ring assembly (Gladfelter *et al.* 2005; Zou *et al.* 2009). The distribution of Bni4 at the neck changes from asymmetric to symmetric along the cell cycle and an increase in its symmetry has been associated with cell cycle arrest (Larson *et al.* 2010); however, the physiological importance of these changes remains unknown.

The genetic correlation analysis of the *bni4*Δ, *slt2*Δ, *pcl1*Δ and *kss1*Δ mutants strongly supports the existence of different physiological roles for Pcl1 and Slt2 kinases, albeit sharing Bni4 as their biological target. While Pcl1 would clearly link Bni4 to septin function, Slt2 would instead link Bni4 to cytoskeletal organization (Figure 7, see shaded boxes). Not surprisingly, both pathways are integrated in Swe1, the master regulatory element in the cytokinesis checkpoint and thus a critical counterpart in septum assembly. By contrast, genetic correlation with Kss1 is almost null, highlighting its minimal functional role in septum assembly, which was only uncovered by means of overexpression. Regardless of the precise functions of Slt2 and Bni4 in septum assembly, which remain to be determined, what is becoming clear is that Bni4 distribution at the neck is linked to its phosphorylation status, which depends not only on Pho85 cyclin-dependent kinases, as previously reported (Zou *et al.* 2009), but also on the Slt2 MAP kinase, as demonstrated throughout this work. The coordinated action of these kinases on Bni4 would regulate its distribution at the neck, constituting an additional form of linking the yeast cell cycle and morphogenesis. Slt2 would act as a safeguard mechanism for the maintenance of cell integrity at the neck (Harrison *et al.* 2001), acting directly by phosphorylating Bni4. The coordination between this signal and that of Pcl1 would be extremely fast and could constitute a "fine tuning" mechanism for the stronger functional relationship between both kinases previously shown to occur through the SBF complex (Madden *et al.* 1997).

ACKNOWLEDGMENTS

Special thanks are due to J. Arroyo and M.A de la Torre for providing strains, plasmids and reagents; to R.Valle for technical assistance, and to N. Skinner for language revision.

FUNDING

This research was supported by grants BFU2010-18632 and BFU2013-48582-C1 from the Spanish Ministry of Science and Innovation (Madrid, Spain). JP was partially supported by the JAE-Doc program from the CSIC.

Conflict of interest. None declared.

REFERENCES

Albuquerque, C.P., Smolka, M.B., Payne, S.H, *et al.* A multidimensional chromatography technology for in-depth phosphoproteome analysis.". *Mol. Cell Proteomics* 2008; **7**: 1389-96.

Arcones, I. and Roncero, C. Monitoring chitin deposition during septum assembly in budding yeast. *Methods Mol Biol* 2016; **1369**: 59-72.

Baetz, K., Moffat, J., Haynes, J., *et al.* Transcriptional coregulation by the cell integrity mitogen-activated protein kinase Slt2 and the cell cycle regulator Swi4. *Mol Cell Biol* 2001; **21**: 6515-28.

Bulik, D.A., Olczak, M., Lucero, H.A., *et al.* Chitin synthesis in Saccharomyces cerevisiae in response to supplementation of growth medium with glucosamine and cell wall stress. *Eukaryot Cell* 2003; **2**: 886-900.

Cabib, E. and Schmidt, M. Chitin synthase III activity, but not the chitin ring, is required for remedial septa formation in budding yeast. *FEMS Microbiol Lett* 2003; **29**: 299-305.

Castrejon, F., Gomez, A., Sanz, M., *et al.* The RIM101 pathway contributes to yeast cell wall assembly and its function becomes essential in the absence of mitogen-activated protein kinase Slt2p. *Eukaryot Cell* 2006; **5**: 507-17.

Chen, R.E. and Thorner, J. Function and regulation of MAPK signaling pathways: Lessons learned from the yeast *Saccharomyces cerevisiae*. *Biochem Biophys Acta* 2007; **1773**: 1311-40.

Chi, A., Huttenhower, C., Geer, L.Y., *et al.* Analysis of phosphorylation sites on proteins from Saccharomyces cerevisiae by electron transfer dissociation (ETD) mass spectrometry. *Proc Natl Acad Sci U S A.* 2007: 2193-98.

Cos, T., Ford, R. A., Trilla, J.A., *et al.* Molecular analysis of Chs3p participation in chitin synthase III activity. *Eur. J. Biochem.* 1998; **256**: 419-26.

DeMarini, D.J., Adams, A.E.M., Fares, H., *et al.* A septin-based hierarchy of proteins required for localized deposition of chitin in the *Saccharomyces cerevisiae* cell wall. *J. Cell Biol.* 1997; **139**: 75-93.

Foiani, M., Marini, F., Gamba, D., *et al.* The B subunit of the DNA polymerase alpha-primase complex in Saccharomyces cerevisiae executes an essential function at the initial stage of DNA replication. *Mol Cell Biol* 1994; **14**: 923-33.

Fung, K.Y., Dai, L., and Trimble, W.S. Cell and molecular biology of septins. *Int Rev Cell Mol Biol* 2014; **310**: 289-339.

García, R., Rodríguez-Peña, J.M., Bermejo, C., *et al.* The high osmotic response and cell wall integrity pathways cooperate to regulate transcriptional responses to zymolyase-induced cell wall stress in Saccharomyces cerevisiae. *J Biol Chem* 2009; **284**: 10901-11.

Gladfelter, A.S., Kozubowski, L., Zyla, T.R., *et al.* Interplay between septin organization, cell cycle and cell shape in yeast. *J Cell Sci* 2005; **118**: 1617-28.

Gomez, A., Perez, J., Reyes, A., *et al.* Slt2 and Rim101 contribute independently to the correct assembly of the chitin ring at the budding yeast neck in *Saccharomycces cerevisiae*. *Eukaryot. Cell* 2009; **8**: 1449-559.

Harrison, J.C., Bardes, E.S., Ohya, Y., *et al.* A role for the Pkc1p/Mpk1p kinase cascade in the morphogenesis checkpoint. *Nat Cell Biol.* 2001; **3**: 417-20.

Hruby, A., Zapatka, M., Heucke, S., *et al.* A constraint network of interactions: protein-protein interaction analysis of the yeast type II phosphatase Ptc1p and its adaptor protein Nbp2p. *J Cell Sci* 2011; **124**: 35-46.

Jung, U.S., Sobering, A.K., Romeo, M.J., *et al.* Regulation of the yeast Rlm1 transcription factor by the Mpk1 cell wall integrity MAP kinase. *Mol Microbiol* 2002; **46**: 781-89.

Kim, K.Y., Cosano, I.C., Levin, D.E., *et al.* Dissecting the transcriptional activation function of the cell wall integrity MAP kinase. *Yeast* 2007; **24**: 335-42.

Kozubowski, L., Panek, H., Rosenthal, A., *et al.* A Bni4-Glc7 phospatase complex that recruit chitin synthase to the site of bud emergence. *Mol. Biol. Cell.* 2003; **14**: 26-39.

Kunkel, T.A., Roberts, J.D., and Zakour, R.A. Rapid and efficient site-specific mutagenesis without phenotypic slection. *Methods in Enzymology* 1987; **154**: 367-82.

Larson, J.R., Kozubowski, L., and Tatchell, K. Changes in Bni4 localization induced by cell stress in Saccharomyces cerevisiae. *J Cell Sci* 2010; **123**: 1050-59.

Larson, J.R., Bharucha, J.P., Ceaser, S., *et al.* Protein Phosphatase Type 1 Directs Chitin Synthesis at the Bud Neck in Saccharomyces cerevisiae. *Mol Biol Cell* 2008; **19**: 3040-51.

Lee, B.N. and Elion, E.A. The MAPKKK Ste11 regulates vegetative growth through a kinase cascade of shared signaling components. *Proc Natl Acad Sci U S A.* 1999; **96**: 12679-84.

Lesage, G., Shapiro, J., Specht, C.A., *et al.* An interactional network of genes involved in chitin synthesis in Saccharomyces cerevisiae. *BMC Genet* 2005; **6**: 8.

Levin, D.E. Regulation of cell wall biogenesis in Saccharomyces cerevisiae: the cell wall integrity signaling pathway. *Genetics* 2011; **189**: 1145-75.

Li, X., Ferro-Novick, S., and Novick, P. Different polarisome components play distinct roles in Slt2p-regulated cortical ER inheritance in Saccharomyces cerevisiae. *Mol Biol Cell* 2013; **24**: 3145-54.

Madden, K., Sheu, Y.J., Baetz, K., *et al.* SBF cell cycle regulator as a target of the yeast PKC-MAP kinase pathway. *Science* 1997; **275**: 1781-84.

Madhani, H.D., Styles, C.A., and Fink, G.R. MAP kinases with distinct inhibitory functions impart signaling specificity during yeast differentiation. *Cell* 1997; **91**: 673-84.

Oh, Y. and Bi, E. Septin structure and function in yeast and beyond. *Trends Cell Biol.* 2011; **21**: 141-8.

Pérez, J., Gómez, A., and Roncero, C. Upregulation of the PRB1 gene in the Saccharomyces cerevisiae rim101Delta mutant produces proteolytic artefacts that differentially affect some proteins. *Yeast* 2010; **27**: 575-81.

Roemer, T., Vallier, L., Sheu, Y.J., *et al.* The Spa2-related protein, Sph1p, is important for polarized growth in yeast. *J Cell Sci* 1998; **111**: 479-94.

Roncero, C. and Sanchez, Y. Cell separation and the maintenance of cell integrity during cytokinesis in yeast: the assembly of a septum. *Yeast* 2010; **27**: 521-30.

Rose, M.D., Wisnton, F. , and Hieter, P. (1990), *Methods in Yeast Genetics: A Laboratory Course Manual.* (New York: Cold Spring Harbor Laboratory Press).

Sacristán-Reviriego, A., Martín, H., and Molina, M. Identification of putative negative regulators of yeast signaling through a screening for protein phosphatases acting on cell wall integrity and mating MAPK pathways. *Fungal Genet Biol* 2015*;* **77**: 1-11.

Sambrook, J. , Fritsch, E. F., and Maniatis, T. Molecular Cloning: A laboratory manual. *Cold Spring Harbor laboratory press* 1989.

Sanz, M., Castrejon, F., Duran, A.*, et al.* Saccharomyces cerevisiae Bni4p directs the formation of the chitin ring and also participates in the correct assembly of the septum structure. *Microbiology* 2004*;* **150**: 3229-41.

Schmidt, M., Varma, A., Drgon, T.*, et al.* Septins, under Cla4p regulation, and the chitin ring are required for neck integrity in budding yeast. *Mol. Biol. Cell* 2003*;* **14**: 2128-41.

Schwartz, M.A. and Madhani, H.D. Principles of MAP kinase signaling specificity in Saccharomyces cerevisiae. *Annu Rev Genet* 2004*;* **38**: 725-48.

Sheu, Y.J., Barral, Y., and Snyder, M. Polarized growth controls cell shape and bipolar bud site selection in Saccharomyces cerevisiae. *Mol Cell Biol* 2000*;* **20**: 5235-47.

Tahirovic, S., Schorr, M., Then, A.*, et al.* Role for lipid signaling and the cell integrity MAP kinase cascade in yeast septum biogenesis. *Curr Gen* 2003*;* **43**: 71-78.

van Drogen, F. and Peter, M. Spa2p functions as a scaffold-like protein to recruit the Mpk1p MAP kinase module to sites of polarized growth. *Curr Biol* 2002*;* **12**: 1698-703.

Zou, J., Friesen, H., Larson, J.*, et al.* Regulation of cell polarity through phosphorylation of Bni4 by Pho85 G1 cyclin-dependent kinases in Saccharomyces cerevisiae. *Mol Biol Cell* 2009*;* **20**: 3250-59.

Table 1. Yeast strains and Plasmids used throughout the work

Strain	Relevant genotype	Source
FCM10	W303 *MATa*	Laboratory collection
FCM314	W303 *MATa rim101::kanMX4*	Castrejon, *et al*. (2006)
FCM500	W303 *MATa rim101::kanMX4 slt2::natMX4*	This study
FCM499	W303 *MATa slt2::NatMX4*	This study
FCM139	W303 *MATa kss1::URA3*	This study
FCM795	W303 *MATa slt2::NatMX4 kss1::URA3*	This study
Y1783	*MATa ura3-52 leu2-3,112 trip1-1 his4 canR*	Cid *et al*. (1998)
CRM818	Y1783 *MATα cdc10-11*	Cid *et al.* (1998)
CRM821	Y1783 *MATα cdc10-11 bni4:: URA3*	Sanz *et al.* (2004)
CRM811	Y1783 *MATα cdc10-11 slt2::natMX4*	This study
CRM3014	W303 *MATa KSS1-GFP::natMX4*	This study
Plasmids		
FCM494	YEp13::*CCT7*	Gómez *et al*. (2009)
FCM576	YEp13::*SPH1*	Gómez *et al*. (2009)
FCM492	YEp13::*PCL1*	Gómez *et al*. (2009)
FCM493	YEp13::*GFA1*	Gómez *et al*. (2009)
FCM486	YEp13::*KSS1*	Gómez *et al*. (2009)
FCM493	pRS424**::***GFA1*	Gómez *et al*. (2009)
CRM874	pRS314*::CDC3-GFP*	Gómez *et al*. (2009)
FCM573	pRS424**::***KSS1*	This study
FCM574	pRS426*::KSS1*	This study
CRM2992	pRS426*::KSS1-GFP*	This study
FCM684	YEp352::*FUS3*	Santos *et al*. (2007)
FCM685	YEp352*:GAL1-KSS1*	Laboratory collection
FCM686	YEp352*::GAL1-KSS1*^{K42R}	Laboratory collection
FCM682	YEp352-*HOG1*	Laboratory collection
CRM951	pRS314*::BNI4-YPF*	This study
FCM689	pRS314*::BNI4*^{S364A}*-YPF*	This study
FCM690	pRS314*::BNI4*^{T427A}*-YPF*	This study
FCM691	pRS314*::BNI4*^{T443A}*-YPF*	This study
FCM693	pRS314*::BNI4*^{T769A}*-YPF*	This study
FCM688	pRS314*::BNI4-3xHA*	This study
FCM424	pUG35 *Slt2-GFP*	MA de la Torre
FCM423	YEp352-*MLP1-LacZ*	García *et al*. (2009)

FIGURE LEGENDS

Figure 1. Multicopy suppression of the synthetic lethality (SL) of *slt2*Δ *rim101*Δ mutant. (A) The mutant strains transformed with multicopy plasmids containing the different suppressors as indicated were grown at 28 ºC on the indicated media. Note that all the transformed strains, but not the control, were able to grow on plain YEPD to different extents. (B) Calcofluor staining of the indicated stains in osmotically supplemented media. Note the increased levels of staining caused by *GFA1*, but not by *KSS1*, overexpression. (C) Neck localization of Bni4-YFP in the indicated strains. *KSS1*, but not *GFA1*, increases the levels of double rings at the neck. Numerical values indicate the percentage of cells containing double Bni4-YFP rings at the neck (n>60). * indicates values significantly different from the wild-type ($p<0.05$)

Figure 2. Suppression of *slt2*Δ phenotypes by *KSS1* overexpression. (A) Growth of the *slt2*Δ mutant transformed with multicopy plasmids containing the indicated genes. Cells were grown in SD selective media for each plasmid, plated on complete SD media with glucose or galactose as carbon source, and incubated at the indicated temperatures for 3 days. $KSS1^{K42R}$encodes a catalytically inactive version of this MAP kinase. (B) Growth of the indicated stains in the presence of increased concentration of Zymolyase. See Materials and methods for experimental details. (C) Localization of Bni4-YFP in the indicated strains. Numbers indicate the percentage of cells showing symmetric rings of Bni4-YFP at the neck, (*) indicates values significantly different from the wild-type ($p<0.05$). (D) β-Galactosidase levels promoted by the *MPL1-LacZ* construct in the wild-type and *slt2*Δ strains with or without the pRS424-*KSS1* plasmid. Activity was assessed as described in Experimental Procedures (C), and after cell wall damage produced by Zymolyase (Z) or calcofluor (CW) treatment. The values represent the average of three independent experiments.

Figure 3. Phenotypic characterization of the *kss1*Δ mutant. (A) Localization of Kss1-GFP, either integrated at the genome (upper) or after overexpression (lower). Note its partial localization at the neck (arrowheads). (B) Comparative growth of the indicated strains in YEPD media supplemented as indicated. (C) Vital calcofluor staining of the indicated strains. Note the normal levels of fluorescence shown by the *kss1*Δ mutant compared with those of the *slt2*Δ mutant. (D) Localization of Bni4-YFP in the wild-type and *kss1*Δ strains. Numbers indicate the percentage of cells showing symmetric rings of Bni4-YFP at the neck. (E) Levels of phosphorylated Slt2 in different strains and after different treatments. Cells were treated with calcofluor for 1 hour as indicated in Materials and Methods. Alternatively, cells were incubated for 60 minutes with α-factor. Western blots were developed with the anti 42/44 antibody to detect the phosphorylated forms of the Slt2, Fus3 and Kss1 MAPK kinases. The unspecific band

(*) is presented as loading control. Note the normal phosphorylation of Slt2 in the *kss1*Δ mutant, but also the absence of phosphorylated forms of Kss1 and Fus3 in the *slt2*Δ mutant.

Figure 4. Characterization of the SL of the *slt2*Δ *kss1*Δ mutant. (A) Growth of the indicated strains in different media. (B) Microscopic aspect of the indicated strains in media with or without sorbitol. Cells were grown in SD-Sorbitol and transferred to SD ± sorbitol as indicated for 3 hours. Note the extensive lysis of the *slt2*Δ *kss1*Δ strain without sorbitol and the presence of aberrant septa (arrowheads). (C) Average values in micrometers of diameters of the rings formed by Bni4-YFP, Cdc3-GFP or chitin at the neck in the indicated strains. Standard deviations are indicated as well as the statistical significance (* $p<0.05$) of the differences observed ($n>50$). (D) Chitin ring morphology after calcofluor staining of fixed cells (see Material and Methods). (E) Altered morphology of birth and bud scars in the *slt2*Δ *kss1*Δ mutant after vital calcofluor staining in osmotically supplemented medium. Note the very prominent bud scar, but also the narrowed birth scars that lead to pear-shaped daughter cells. Mother (M) and daughter cells (D) are indicated.

Figure 5. Analysis of Bni4 phosphorylation. (A) Bni4-YFP mobility was assessed in SDS-PAGE or Phos-tag™ acrylamide by western blot of total protein extracts. Note in both cases the slightly higher mobility of the protein obtained from the *slt2*Δ mutant strains. Protein was obtained from the indicated strains as described in Materials and Methods. (B) Immunoprecipitated Bni4-YFP obtained from the wild type or *slt2*Δ mutant was treated with alkaline phosphatase (AP) as indicated. Note the increased mobility after AP treatment. (C) Mobility of IP Bni4-YFP after *KSS1* overexpression from pRS424::*KSS1* assessed in SDS PAGE gels. Note the reduced mobility of the protein after *KSS1* overexpression in both the wild-type and *slt2*Δ strains, which was restored to normal levels after the AP treatment. (D) Protein extracts from strains containing Slt2-GFP and/or Bni4-3xHA constructs were immunoprecipitated using the anti-GFP antibody; the resulting protein extracts were separated in SDS PAGE gels and developed by western blot using either anti-GFP (left) or anti-HA antibodies (right). Note the presence of Bni4-3xHA only in the strain co-expressing the Slt2-GFP and Bni4-3xHA proteins. Bni4-3xHA was immunoprecipitated directly from the same strains and visualized with the anti-HA antibody as a loading and size control (right panel). (E) Protein extracts from strains containing pRS426::*KSS1-GFP* and/or pRS314*::BNI4-3xHA* constructs were immunoprecipitated using Anti-GFP MicroBeads; the resulting protein extracts were separated in SDS PAGE gels and developed by western blot using either anti-GFP or anti-HA antibodies as indicated. Note the specific co-immunoprecipitation of Bni4-3xHA with Kss1-GFP.

Figure 6. Phenotypic analysis of the phosphorylatable sites in Bni4. (A) Bioinformatics map of potential phosphorylatable sites on Bni4 (vertical bars). The 11 potential MAPK kinase sites are indicated with the corresponding residues. The sites numbered were chosen for further analysis. (B) Localization of mutated forms of Bni4-YFP. The numbers indicate the percentage of cells showing double Bni4 rings at the neck. Note the reduced number of double rings observed for the Bni4^{T427A} protein. (C) Functionality of the mutated forms of Bni4 in the hypersensitized cells of the *cdc10-11* background. Cells were grown in SD-Trp selective medium, serial-diluted, and plated on the same media. Plates were incubated at 28 ºC and 32 ºC, the permissive and semi-permissive temperatures for the *cdc10-11* mutant. Note that some Bni4 phosphorylatable mutants could not support growth at 32 ºC in the *cdc10-11* background. (D) The indicated strains were transformed with pRS425 or pRS425::*KSS1* and the cells were grown in SD-Leu selective medium and plated on the same medium. Note that the overexpression of *KSS1* partially restored growth at 32 ºC in the *cdc10-11* background in the absence of Slt2 but not of Bni4. (E) Cells of the *cdc10-11 bni4*Δ strains were transformed with the pRS314 plasmid containing the indicated forms of Bni4 and pRS425*::KSS1*, grown in selective SD-Trp-Leu medium to early logarithmic phase, diluted, and plated on the same medium at the indicated temperatures. Note the partial restoration of growth promoted by *KSS1* overexpression in some of the strains. In all cases the images presented in each panel are always from the same set of plates.

Figure 7. Map of genetic correlations between the *SLT2*, *BNI4*, *PCL1* and *KSS1* genes. The genetic correlations (correlation values >0.15) for the different genes were obtained from the Data Repository of Yeast Genetic Interactions (DRYGIN) and compared. Coincidences between the different correlation patterns are shown in the Figure. Note the extensive coincidences between the *BNI4* and *SLT2* correlation patterns, including the complete machinery involved on CSIII, but also several genes functionally linked to cytoskeletal organization. *BNI4* and *PCL1* correlations link through the *SHS1* and *CDC12* septins. The *SLT2*, *BNI4* and *PCL1* correlation patterns coincide only in *SWE1*, a key element in the morphogenesis checkpoint. Note the extremely low level of coincidences of any of these with the *KSS1* correlation pattern.

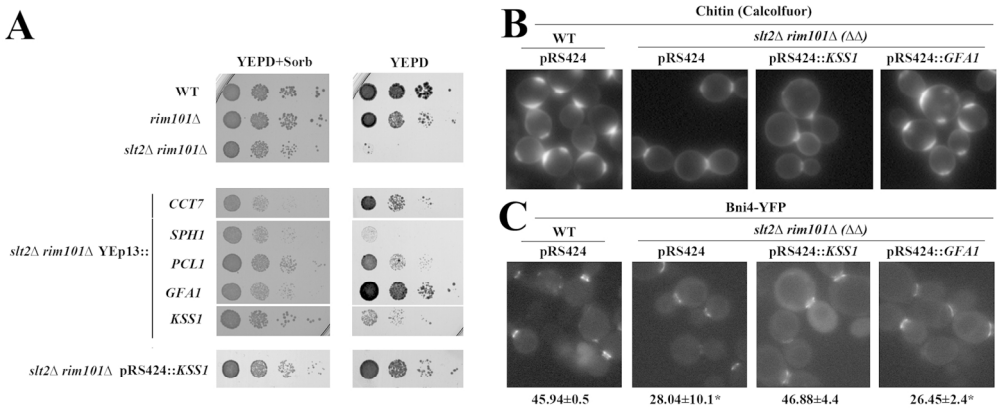

Figure 1

Figure 1
170x80mm (300 x 300 DPI)

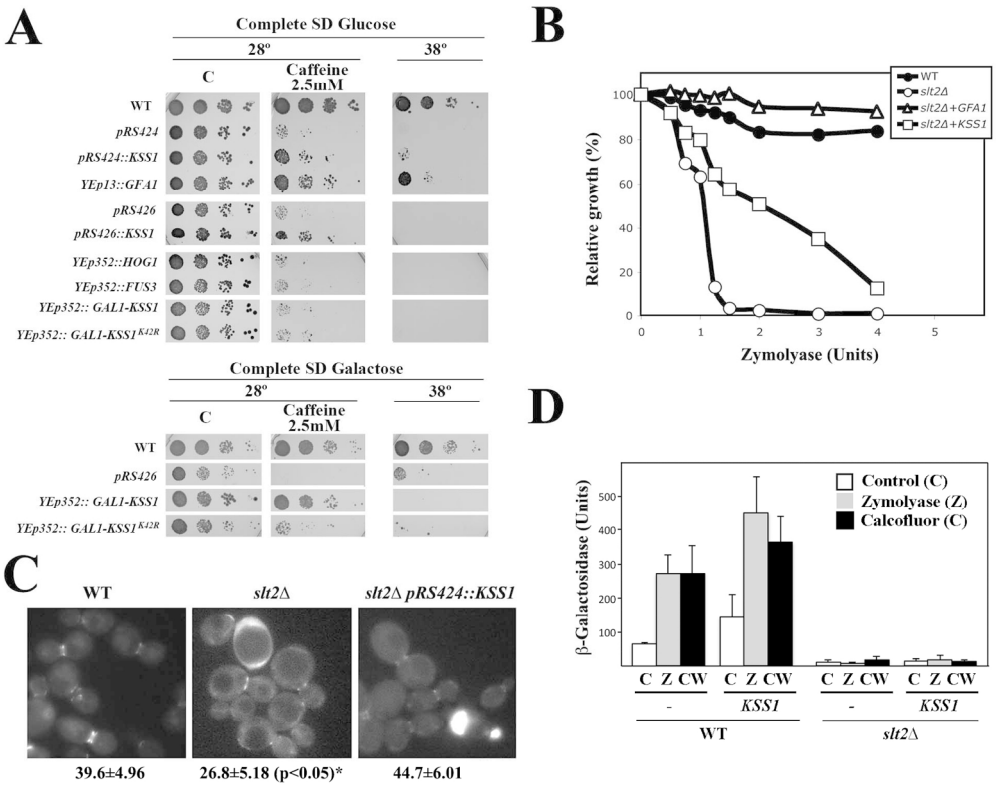

Figure 2

Figure 2
170x144mm (300 x 300 DPI)

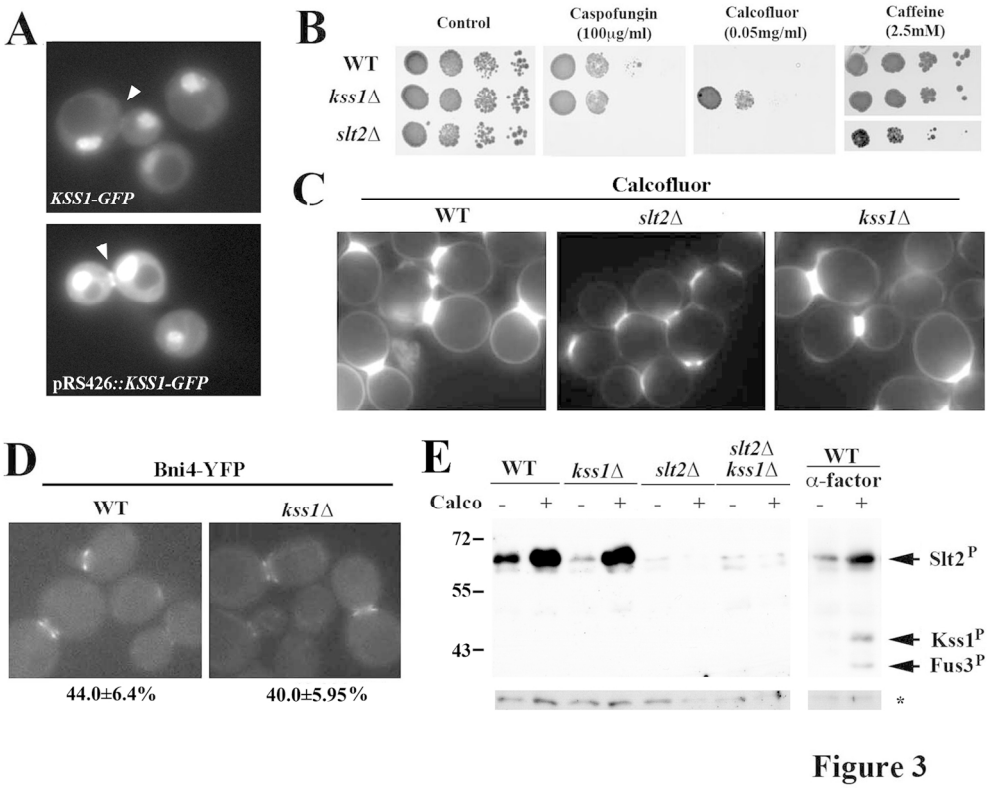

Figure 3

Figure 3
170x138mm (300 x 300 DPI)

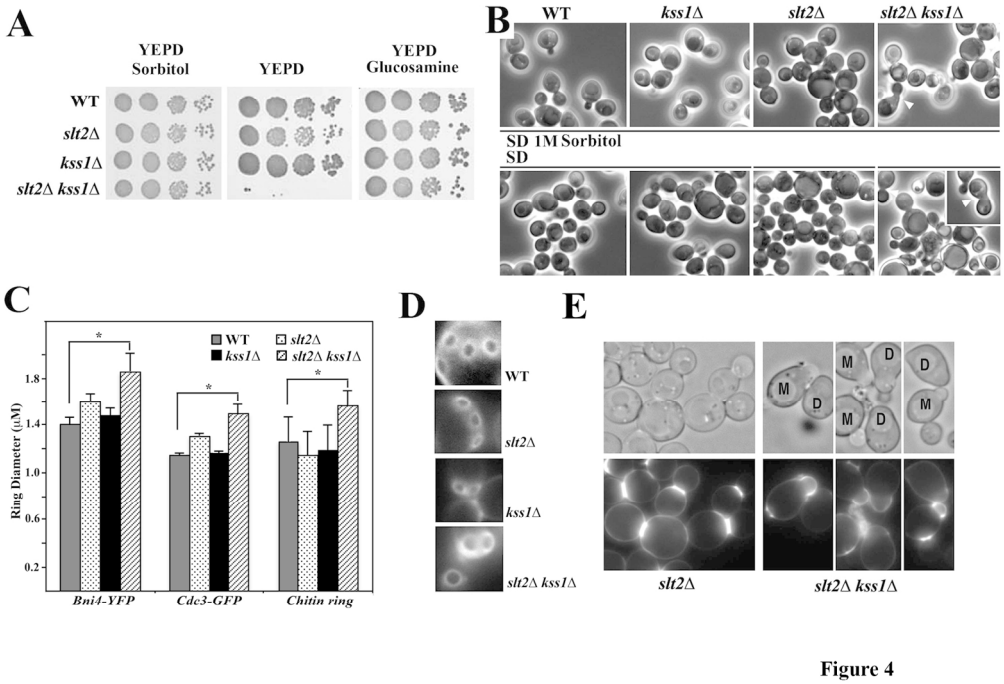

Figure 4

Figure 4
170x119mm (300 x 300 DPI)

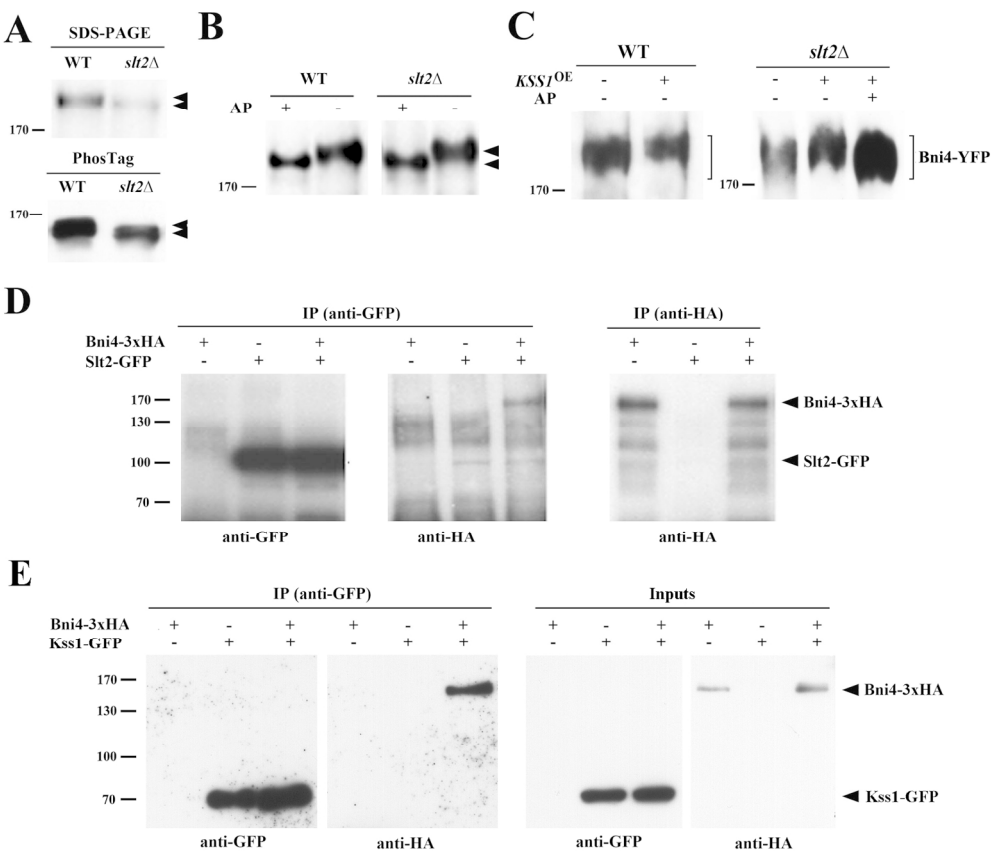

Figure 5

Figure 5
170x161mm (300 x 300 DPI)

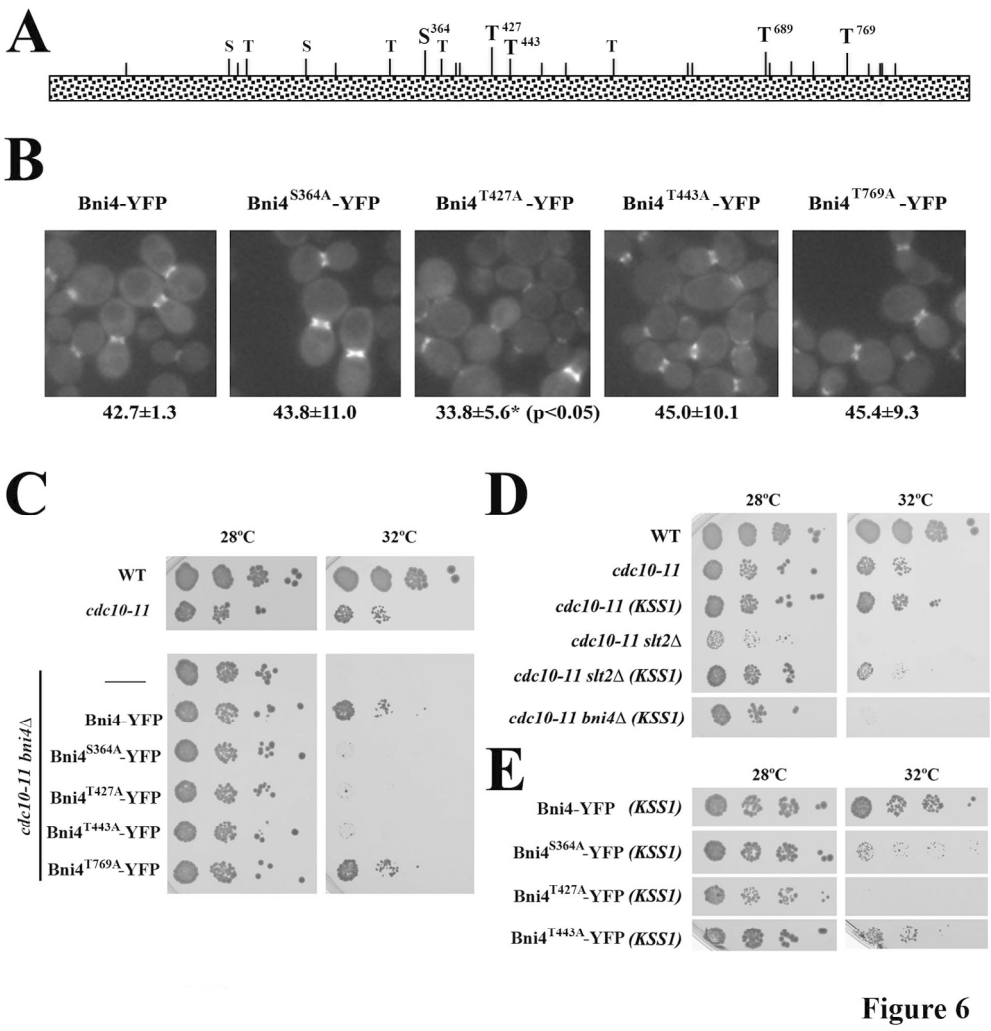

Figure 6

Figure 6
170x175mm (300 x 300 DPI)

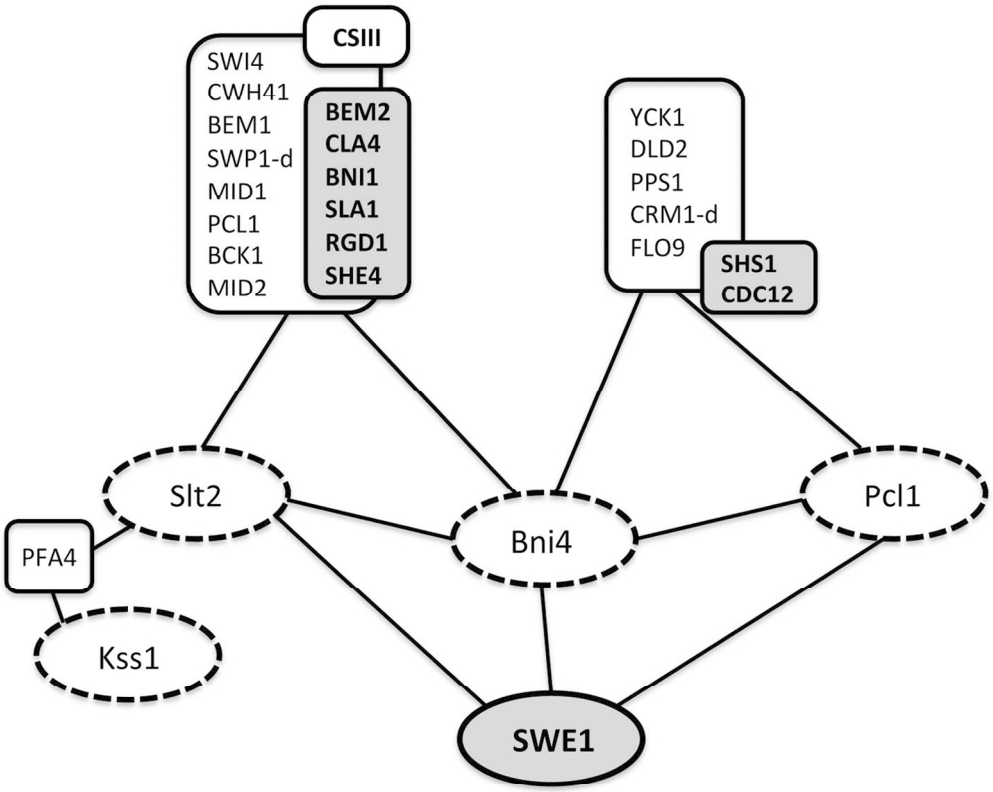

Figure 7

Figure 7
150x132mm (300 x 300 DPI)

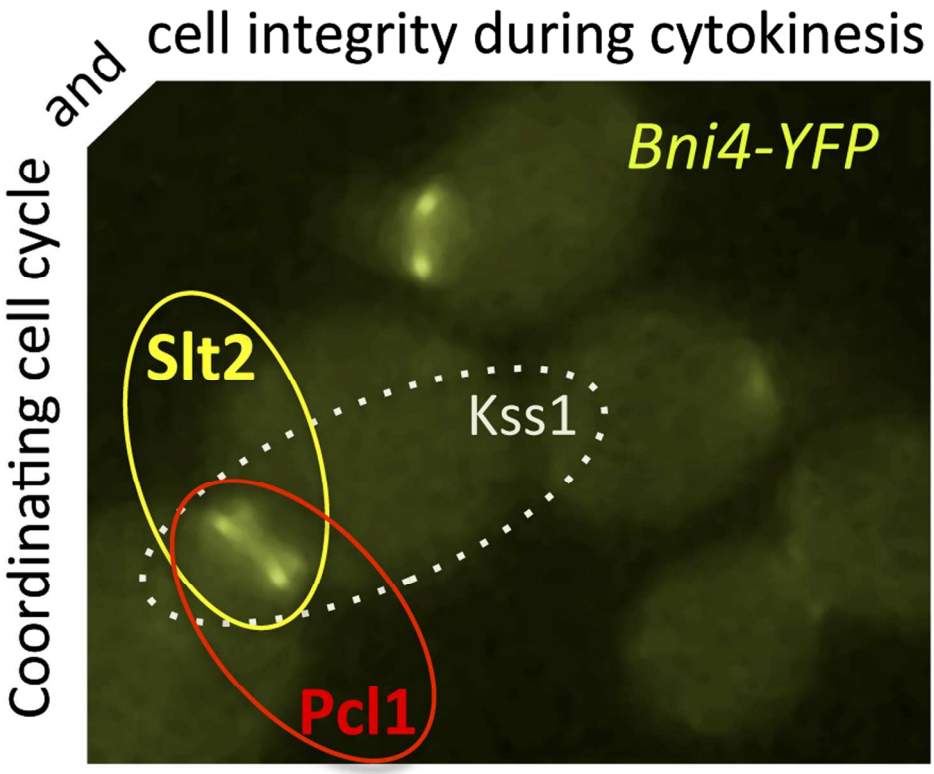

150x122mm (300 x 300 DPI)

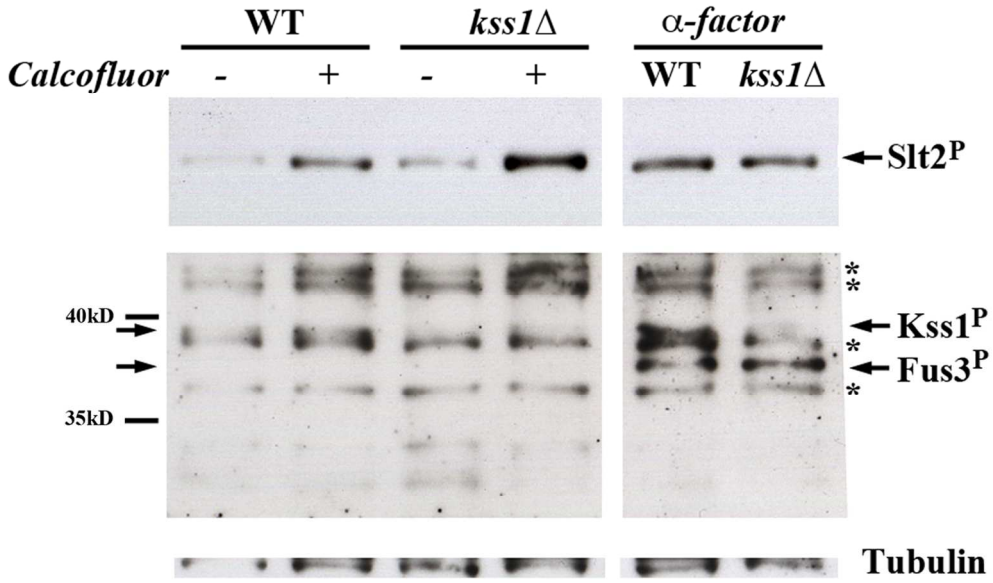

Western blot developed with anti Phospho p42/44. Extracts were obtained from the indicated strains before (-) or after (+) the indicated treatments. Central panel is significantly overexposed in order to show Kss1 and Fus3 bands. Note to the much lower specificity of this batch of antibody compared to the use in the original Figure 3.

119x83mm (300 x 300 DPI)